Nuclear Instruments and Methods in Physics Research A 659 (2011) 373–377

Contents lists available at SciVerse ScienceDirect

Nuclear Instruments and Methods in Physics Research A

journal homepage: www.elsevier.com/locate/nima

Experimental and numerical characterization of the neutron field produced in the n@BTF Frascati photo-neutron source

R. Bedogni [a,*], L. Quintieri [a], B. Buonomo [a], A. Esposito [a], G. Mazzitelli [a], L. Foggetta [a], J.M. Gómez-Ros [a,b]

[a] INFN—LNF (Laboratori Nazionali di Frascati), Via E. Fermi n. 40,00044 Frascati (RM), Italy
[b] CIEMAT, Av. Complutense 22, E-28040 Madrid, Spain

ARTICLE INFO

Article history:
Received 7 July 2011
Received in revised form
1 August 2011
Accepted 16 August 2011
Available online 22 August 2011

Keywords:
Photo-neutrons
FLUKA
MCNPX
Neutron spectrometry
Bonner Sphere Spectrometer
Activation foils
Dysprosium

ABSTRACT

A photo-neutron irradiation facility is going to be established at the Frascati National Laboratories of INFN on the base of the successful results of the n@BTF experiment. The photo-neutron source is obtained by an electron or positron pulsed beam, tuneable in energy, current and in time structure, impinging on an optimized tungsten target located in a polyethylene–lead shielding assembly. The resulting neutron field, through selectable collimated apertures at different angles, is released into a 100 m^2 irradiation room. The neutron beam, characterized by an evaporation spectrum peaked at about 1 MeV, can be used in nuclear physics, material science, calibration of neutron detectors, studies of neutron hardness, ageing and study of single event effect. The intensity of the neutron beam obtainable with 510 MeV electrons and its fluence energy distribution at a point of reference in the irradiation room were predicted by Monte Carlo simulations and experimentally determined with a Bonner Sphere Spectrometer (BSS). Due to the large photon contribution and the pulsed time structure of the beam, passive photon-insensitive thermal neutron detectors were used as sensitive elements of the BSS. For this purpose, a set of Dy activation foils was used. This paper presents the numerical simulations and the measurements, and compares their results in terms of both neutron spectrum and total neutron fluence.

1. Introduction

Fast neutron irradiation facilities are used in many fields, ranging from nuclear physics to radiation protection, material science, telecommunication, electronics, aerospace, defense and plant genetics. Besides neutron reactors and proton and ion accelerators, neutron beams are produced in electron facilities through photo-neutron processes on high-*Z* targets. Examples are Gelina (EC-JRC-IRMM Geel, Belgium) and nELBE (FZD Rossendorf, Germany) [1]. At The Frascati National Laboratories of INFN a photo-neutron irradiation source has been recently set up leading an electron or positron pulsed beam, tuneable in energy, current and in time structure, to impinge an optimized tungsten target located in a polyethylene–lead shielding assembly. The resulting neutron field, through selectable collimated apertures at different angles, is delivered to a 100 m^2 irradiation room. The neutron beam is characterized by an evaporation spectrum peaked at about 1 MeV. Using a 510 MeV electron beam, with time structure of 10 ns pulses at 1 Hz and charge per pulse $\approx$ 50 pC/pulse, the intensity of the neutron beam and its fluence energy distribution at a point of reference in the irradiation room were experimentally measured with a Bonner Sphere Spectrometer (BSS) and simulated with FLUKA and MCNPX Monte Carlo transport codes. The photon spectrum was also simulated.

Due to the large photon contribution and to the pulsed time structure of the beam, passive photon-insensitive thermal neutron detectors were used as sensitive elements of the BSS. For this purpose, a set of Dy activation foils was chosen.

A reference point located at 124 cm height from the floor and at 149 cm from the target center, perpendicularly with respect to the impinging electron beam (90° direction), was chosen for the experiment (see Figs. 1 and 2).

This paper presents the numerical simulations and the measurements, and compares their results in terms of both neutron spectrum and total neutron fluence.

2. The n@BTF field

The BTF (Beam Test Facility) [2,3] is part of the DAΦNE accelerator complex: it is composed of a transfer line, driven of a pulsed magnet that allows diversion of electrons or positrons, normally released to the DAΦNE damping ring, from the high intensity LINAC towards a 100 m^2 experimental hall. The facility

* Corresponding author. Tel.: +39 0694032608; fax: +39 0694035050.
E-mail address: roberto.bedogni@lnf.infn.it (R. Bedogni).

0168-9002/$ - see front matter © 2011 Elsevier B.V. All rights reserved.
doi:10.1016/j.nima.2011.08.032

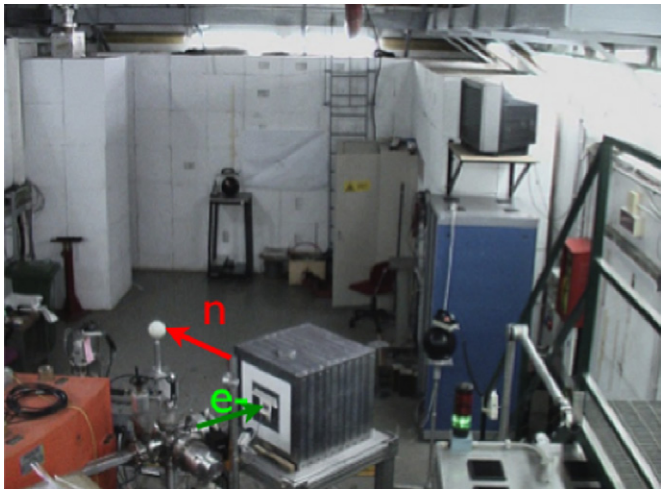

Fig. 1. n@BTF experimental layout.

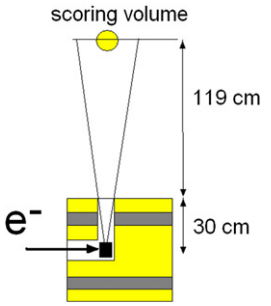

Fig. 2. Simplified scheme of the simulation geometry.

can provide electrons and positrons in a defined range of energy (up to 750 MeV for e^- and 510 MeV for e^+), charge ($<10^{10}$ e/pulse), pulse length (1–10 ns) and injection frequency (<50 Hz). The facility can operate at day and night times, with users coming mainly from Italy (about 50%) and all over Europe.

The n@BTF experiment was realized by dumping high-energy electrons on a properly optimized W target located in a previously studied [4] shielding structure in the BTF experimental hall, as shown in Fig. 1. The photons from the electromagnetic cascade may excite the W nuclei, resulting mainly in neutron production in the MeV region related to the Giant Resonance mechanisms. A few higher-energy neutrons (in the order of %) are expected from the Quasi-Deuteron and photo-pion mechanisms [2].

In order to accurately choose the material and the geometry of the target that maximizes the produced photo-neutrons many cylindrical configurations have been simulated by the Monte Carlo code, changing both the material and linear dimensions (length and radius) of the cylinder.

Several high-Z materials have been chosen as possible optimal candidates for the target: lead, tantalum and tungsten. Among all these materials tantalum and tungsten offer higher neutron yield, for the same target geometry, with respect to lead. Since the neutron yield for Tungsten is only slightly higher than for Tantalum, the final choice between these two materials has been done essentially on the base of thermo-physical properties: tungsten has a thermal diffusivity (which means more effective heat transfer by conduction) almost 3 times larger than that of tantalum.

In the performed simulations all the characteristics of the available electron beam (primary beam energy spread, spot size, energy distribution, etc.) have been taken properly into account. The optimization process has been carried out by estimating for each configuration the neutron fluence leaving the target and the neutron-to-photon fluence ratio in different directions with respect to the incident primary beam. We found that increasing the cylinder length of $5X_0$ (where X_0 is the radiation length of the electromagnetic cascade) from 10 to $15X_0$ would have lead to a corresponding enhancement in neutron yield of about 10%, while for going from $15X_0$ to 20 X_0, the gain would have been less than 3%. So a final cylinder length of $17X_0$ has been chosen (which identified the beginning of the plateau in the neutron yield curve). At the same time a fine-tuning of the final radius has been also performed so that, using the same optimization process, the optimum value for the radius has been determined to be $\simeq 10X_0$ (35 mm). As a result, a cylindrical target with radius 35 mm and length 60 mm was built.

Since the maximum electron beam spot size on the target is enclosed in a circle of 1 cm radius and the accuracy by which we can set the transversal beam size and its center is much better than a few mm, we can be confident that, even in the most disadvantageous case, all the energy of the primary electrons will be deposited in the target. Because the photo-neutron yield depends essentially on the value of the deposited energy, the estimated neutron yield sensitivity with respect to the examined geometrical parameters (beam spot size and radial location of the beam center) is actually negligible (less than 3%).

The lead–polyethylene–lead shield covers almost all the solid angle around the target, leaving only three free paths: the middle square window for the primary electron inlet, and two cylindrical holes for the neutron emission at directions 0° and 90° in a plane perpendicular to the electron beam impinging direction. Whilst the neutron field is practically isotropic, the photon fluence decreases by a factor of 10^2 from the 0° to the 90° direction.

3. Monte Carlo simulations

The FLUKA 2006.3 [5] and MCNPX 2.6 [6] codes were used to determine the neutron or photon fluence and their energy distributions. In FLUKA simulations, the photo-nuclear physics was activated over all the energy range for all the relevant heavy elements included in the model: natural W and Pb. In order to improve the statistics, a biasing technique was used, consisting in increasing the interaction probability of photons by a factor 100 (photon inelastic interaction length λ reduced by a factor 0.01). The neutron fluence per primary particle in the reference point and its energy distribution were estimated using both USRBDX and USRYIELD cards.

According to the FLUKA simulations, the neutron spectrum in the reference point is a Maxwellian-like distribution with peak energy at about 1 MeV and more than 99% of neutrons fluence below 20 MeV.

Concerning MCNPX, the calculations relied on the ENDF/B-VII [7] photo-nuclear data library. The $S(\alpha,\beta)$ data were used for the treatment of the thermal scattering in polyethylene. Both F4 and F5 tallies were used to determine the fluence energy distribution at the points of interest, obtaining coincident results within the simulation uncertainties ($<1\%$). Particularly, the F4 tally was based on a 10 cm diameter scoring sphere centered at the reference point. In the energy range of interest for this work, evaluated cross-section data are scarcely available and the codes rely on nuclear models describing the high-energy inelastic interaction in terms of intra-nuclear cascade (INC), pre-equilibrium and de-excitation models. For MCNPX, the Bertini high-energy interaction model was used.

The same geometry presented in Fig. 2 was adopted for both FLUKA and MCNPX simulations. The neutron and photon spectra are reported in Figs. 3, and 4, and 6, respectively.

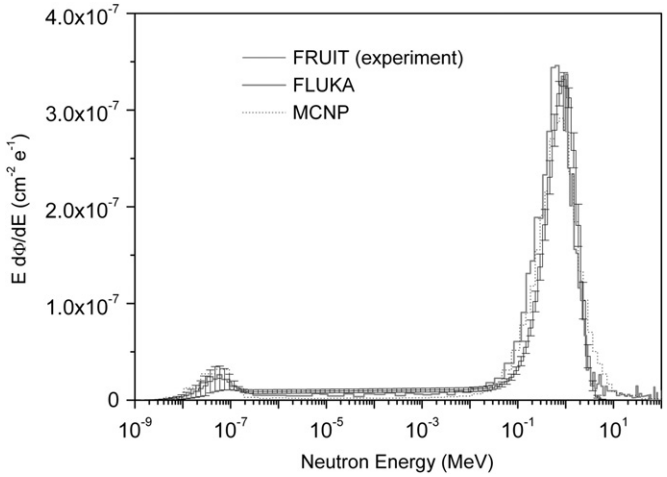

Fig. 3. Comparison between the simulated and experimental neutron spectra over the whole energy range. Uncertainty bars refer to the experimental data (FRUIT unfolding).

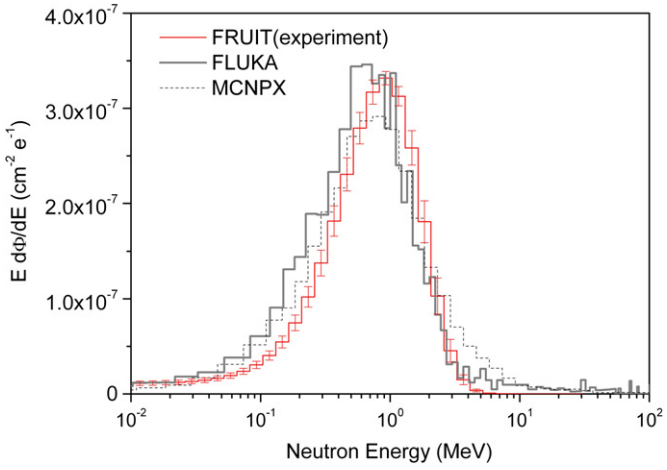

Fig. 4. Comparison between the simulated and experimental neutron spectra in the 0.01–100 MeV energy interval. Uncertainty bars refer to the experimental data (FRUIT unfolding).

The thermal component, representing about 8% of the total fluence, almost exclusively arises from the lead–polyethylene assembly and from the walls and materials contained in the room. The thermal contribution produced within the target is negligible.

4. Dysprosium activation foils-based Bonner Sphere Spectrometer (Dy-BSS)

The BSS equipped with passive detectors is used in accelerator workplaces characterized by high intensity, pulsed time structure, intense photon component and large electromagnetic noise. The passive detectors most suited for electron facilities are certainly the activation foils, due to their insensitivity to photons, to the good knowledge of the cross-sections and to the possibility to perform very precise measurements even with portable counters. Gold [8,9], indium [10] and dysprosium [11,12] foils have been used for this purpose. The Au-BSS exploits the reaction ^{197}Au$(n,\gamma)^{198}$Au and the β-γ emission from ^{198}Au ($T_{1/2}$=2.7d; $E_{\beta\,max}$=0.96 MeV, E_γ=0.41 MeV). In spite of its large use, Au-BSS is characterized by a relatively low response (the specific saturation activity per unit fluence rate is in the order of 0.4 cm^2 g^{-1} for the 8″ sphere at 1 MeV). Its minimum detectable fluence rate was found to be in the order of 10^3–10^4 cm^{-2} s^{-1} [13], depending on the foil dimensions, neutron spectrum, exposure time, exposure to counting delay and counting time. Increasing the foil thickness and diameter can lower this figure, but this would also increase self-absorption and anisotropy effects.

Indium foils, exploiting the reaction ^{115}In$(n,\gamma)^{116m}$In and the β-γ emission from ^{116m}In ($T_{1/2}$=54 min; $E_{\beta\,max}$=0.6 MeV −1.0 MeV; E_γ=0.4–1.3 MeV), have been also used. The counting rate is much higher than for gold foils, but the very short half-life may constitute a serious limitation for operational measurements.

Dysprosium foils probably constitute the optimal compromise for operational measurements. The exploited isotope is ^{164}Dy (28.2% abundance in natural dysprosium). ^{165}Dy is a β–γ emitter with $E_{\beta\,max}$=1.3 MeV and $T_{1/2}$=2.334 h. The cross-section is significantly higher than that of gold (~2700 b at thermal energy, to be compared with the 98.8 b of ^{197}Au).

The Dy-BSS used in this work is based on foils with 12 mm diameter and 0.1 mm thickness that are analyzed with a portable beta counter. The impact of parasitic (n,γ) and (γ,n) reactions on the beta counting has been investigated in different neutron fields, including high-energy fields, and no significant perturbations have been found. The Dy-BSS response matrix was calculated with MCNPX on the basis of a 68-group energy equi-lethargy structure from 1.5E−9 MeV to 1.16E+3 MeV. A validation experiment performed in the ENEA-Bologna ^{252}Cf reference field allowed estimating the response matrix overall uncertainty to ±2.3%. This figure refers to the energy interval covered by the ^{252}Cf spectrum, i.e. from 0.1 to 15 MeV.

Details about the response matrix and its experimental validation are given in Ref. [11]. Recently this system and its extension to a single-sphere activation spectrometer were successfully tested in neutron fields from a spallation source [12,14] and from a fusion-based generator [15].

Because the response matrix of the Dy-BSS is defined in terms of saturation specific activity (or saturation count rate in the beta counter) per unit neutron fluence rate as a function of the neutron energy and of the sphere dimension, the result of a foil counting should be corrected for the following effects before its use in the unfolding code: (1) the detector background and efficiency, (2) the decay between the end of the irradiation and the beginning of the measurement, (3) the decay during the measurement and (4) the fraction of the saturation activity reached during the irradiation. The latter (saturation factor F_{sat}) is given, for constant rate sources, by :

$$F_{sat} = 1 - 2^{-t_{irr}/T} \quad (1)$$

where t_{irr} is the irradiation time and T the half-life of the isotope. In the present experiment this formula could not be used because the neutron source was pulsed and because each pulse differed from the others in terms of delivered charge, with a variability as large as 15% (one s.d.). The F_{sat} was therefore calculated on the basis of a pulse-by-pulse discrete calculation [15], relying on the indication of a charge monitor.

5. Experiment

The energy distribution of the incident electrons was measured by a spectrometer consisting of a pulsed magnet, which deviates the beam from the Transfer Line, and a 60° bending magnet, which focuses the beam on a system of secondary emission metallic strips [16]. The FHWM of this distribution is lower than 1%.

To measure the charge and transverse profile of the beam delivered on the tungsten target, a Bergoz ICT (high sensitivity,

beam charge to output charge ratio 5:1) and two fluorescent screens (beryllium oxide and YAG:Ce) were mounted at the exit of the line. The Integrating Current Transformer (ICT) is a capacitively shorted transformer and a fast read out transformer in a common magnetic circuit designed to measure the charge in a very short pulse with high accuracy.

Variations in the neutron fields due to small instabilities in the electron beam were minimized by keeping the beam position and beam spot dimensions as constant as possible. These parameters can be easily checked and controlled using wall current monitors and fluorescent targets suitably located along the BTF transfer line.

The repeatability of the neutron beam directional distribution was checked using two neutron ambient survey-meters of types Berthold LB64-11 and ALNOR 2002B, having energy interval of the response from thermal up to 20 MeV neutrons. These instruments were placed at about 7 m from the target along two different directions (0° and 90° with respect to the direction of the incident electrons). The ratio of their readings remained constant (within $\sigma_{dir} \pm 1.5\%$) during the irradiation period, thus indicating a satisfactory repeatability of the irradiation conditions.

The spheres with Dy activation foils in their center were sequentially exposed at the reference point (149 cm from the target center along the 90° direction at 124 cm from the floor) for an irradiation time of around 0.5 h for each sphere. The delivered charge per pulse was about 50 pC. The following spheres were exposed: 2″, 3″, 5″, 7″, 8″, 10″, 12″. Extended range spheres [17] were not used because the expected fraction of neutron fluence above 20 MeV is only 0.4%. In addition the (γ,n) reactions induced by high-energy photons in the metal layer of the extended range spheres could produce extra neutrons, possibly leading to an undesired increase of the Dy foils activity.

In order to limit the sources of uncertainty to the maximum extent and to guarantee reproducible irradiation condition for all spheres, the following aspects were considered:

1) Determination of the saturation factor F_{sat} on the basis of a "shot-to-shot" calculation, see Section 4.
2) The overall uncertainty of the Dy-BSS response matrix, estimated from previous validation experiments, was taken into account, $\sigma_{mat} = \pm 2.3\%$.
3) Variations in the neutron fields due to small instabilities in the beam were considered on experimental basis (see above), obtaining an uncertainty figure of $\sigma_{dir} = \pm 1.5\%$.
4) A computational analysis was performed with MCNPX to understand the influence of small positioning errors in the total neutron fluence at the reference point. The results are shown in Table 1. Since the estimated positioning error in this experiment was < 1 cm, an associated uncertainty $\sigma_{pos} = 1\%$ was considered for the fluence estimation.

The foils were counted in a portable beta counter; their specific activity was corrected for the discrete activation function, the decay from the exposure and the counting, and the decay during counting, and finally normalized to the number of 510 MeV electrons delivered to the target. These values were unfolded using the FRUIT code [18,19]. The neutron spectrum, in equi-lethargy representation, is shown in Fig. 3 together with the spectra calculated with MCNPX and FLUKA in the whole energy interval, from thermal up to 100 MeV neutrons. To better compare the results in the interval where the evaporative peak is located, the same curves have been restricted to the 0.01–100 MeV interval (see Fig. 4). Both plots indicate a good agreement between experiment and simulations.

Fig. 4 shows the experimental uncertainties for every energy bin, obtained in FRUIT by propagating the uncertainty affecting the input data (quadratic combination of uncertainties of foil measurements, beam stability σ_{dir}, response matrix σ_{mat}) on the output spectrum through a statistical analysis involving a large number of automatic unfolding processes using perturbed sets of foil activities. They range from 5% to 20%, which is a consequence of the limited energy resolution of the Bonner Sphere Spectrometer. It is also important to mention that the BSS provides no information above 20 MeV, due to the impossibility to use metal-loaded extended range spheres in this experiment. It should be underlined that the differences, observed in Figs. 3 and 4, between the experimental values and the Monte Carlo predictions and between the two code simulations, are fully acceptable for the purposes of this work. These differences must be judged with the awareness that the neutron spectra are examined over ten orders of magnitude and that the BSS is the only instrument able to measure a spectrum with such extension in energy. Very similar considerations were drawn in an EU-CONRAD high-energy comparison, performed in the neutron spectrum induced by a 400 MeV/*A* carbon ion on a graphite target [20].

The FRUIT code models the neutron spectrum as the superposition of elementary functions parameterized by parameters with physical meaning. Particularly, the "evaporation" model describes the evaporation peak as a Maxwellian function with temperature *T*, corresponding to half the peak energy. The probability distribution for *T* (see Fig. 5), derived by FRUIT, shows that the most probable peak energy is 0.9 MeV, whilst the 95% confidence interval ranges from 0.7 to 1.1 MeV. This result fully agrees with the numerical predictions (see Section 3).

A quantitative comparison between measurements and simulations can be done on the basis of Table 2, where the total neutron fluence at the reference point per unit incident electron is

Table 1
Total neutron fluence in the reference point from the experiment and the simulations. Uncertainties refer to one sigma.

Distance variation (cm)	$(\Phi - \Phi_o)/\Phi_o$(%)
−3	+4
−2	+3
−1	+1
0	0
+1	−1
+2	−3
+3	−4

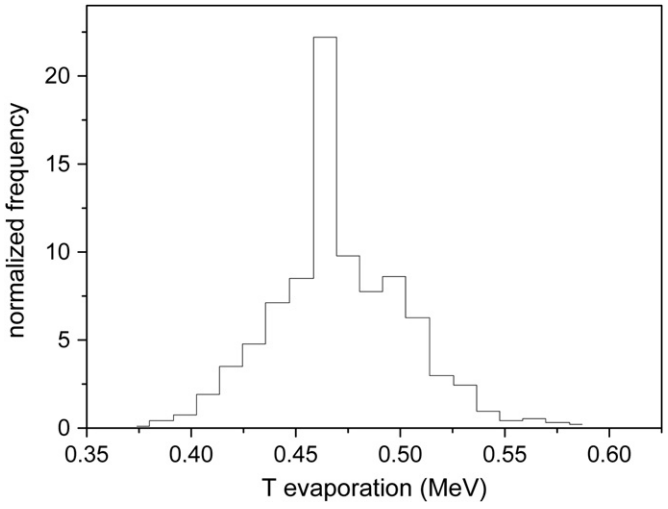

Fig. 5. Probability distribution for the evaporation temperature derived by the FRUIT code.

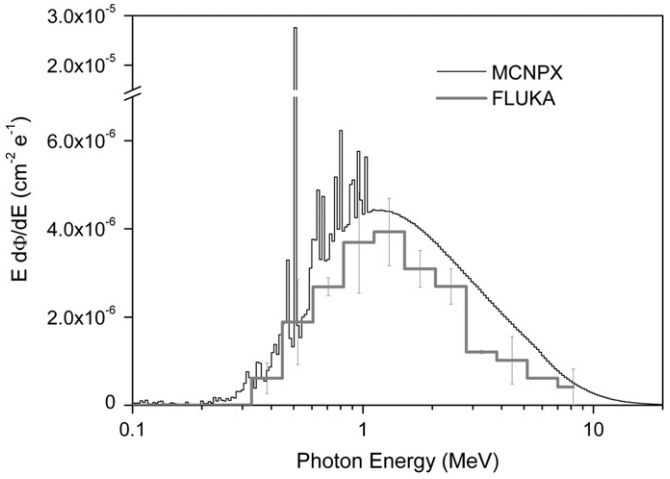

Fig. 6. Photon spectra at the point of test calculated by MCNPX and FLUKA. The spectra are normalized per unit incident electron of the target and in equi-lethargy representation. The total fluence is $1E-5\,cm^{-2}$ per electron. The fraction of fluence above 10 MeV is 0.7%. Due to differences in the hardware resources, the uncertainties in the FLUKA spectrum (10%–20%) are higher than those in the MCNPX calculations (1%–2%).

Table 2
Result of the sensitivity analysis carried out to determine the variation in the neutron fluence due to small variations in the instrument positioning.

	Neutron fluence per incident electron $\Phi(10^{-7}\,cm^{-2})$
FRUIT (experiment)	8.04 ± 0.25
FLUKA	8.12 ± 0.04
MCNPX	(Tally F4) 8.06 ± 0.04
	(Tally F5) 8.020 ± 0.002

shown. Here the experimental uncertainty is much lower than that related to the energy bins in the spectrum. It is a known fact that well-established BSS can measure spectrum-integrated quantities with accuracy better than 5% [20]. The uncertainty of the experimental fluence ($\pm 3.1\%$) comes from the quadratic combination of the uncertainty in the calibration factor of the Dy-BSS ($\pm 2.3\%$), the unfolding uncertainty ($\pm 1.9\%$) and the positioning uncertainty σ_{pos} ($\pm 1\%$).

An independent confirmation of the fluence data comes from the experimental formula of Swanson [21], giving the fast neutron fluence (energies higher than approximately 10 keV) per unit electron incident on thick targets. This provides $6.85 \times 10^{-7}\,cm^{-2}$ (10% uncertainty can be assumed), which is comparable with the experimental value from this work of $(6.53 \pm 0.20) \times 10^{-7}\,cm^{-2}$.

6. Conclusions

The numerical and experimental work described in this paper allowed an accurate characterization of the n@BTF neutron beam in terms of total neutron fluence and its energy distribution. Two independent FLUKA and MCNPX models of the irradiation assembly were built, and the neutron spectra in the reference points were calculated using the state-of-art photo-neutron physics implemented in the codes. The same predicted values (within uncertainties) of total neutron fluence were obtained and the simulated spectra obtained with the previously cited Monte Carlo codes are in good agreement, with limited differences ascribable to different cross-section libraries and photo-nuclear models. The neutron spectrum was measured with a well-established Bonner Sphere Spectrometer equipped with dysprosium activation foils. The experimental results are in agreement with the simulations, taking into account the limitations due to the modest energy resolution of the spectrometer and to the impossibility to use extended range metal-loaded spheres. Further investigations are foreseen, in the direction of developing a photon-insensitive high-energy spectrometer to accurately measure also the high-energy component of the neutron spectrum (20 MeV and above).

The n@BTF beam can be used in nuclear physics, material science, calibration of neutron detectors, studies of neutron hardness, ageing and study of single event effect. Particularly, due to the short pulse length (1–10 ns) and to the possibility of setting up flight paths of a few meters length, time-of-flight measurements with good energy resolution up to the keV region could be performed for material science (for a flight path of 2 m and a pulse duration of 10 ns, $\Delta E/E \approx 1\%$ at 10 keV and 4% at 100 keV). In addition, n@BTF could be used to test the performance of neutron dosimetry instruments to be employed in pulsed fields such as those encountered in laser-based accelerator facilities.

Aknowledgments

This work has been partially supported by the INFN - CSN5 (*Commissione Scientifica* Nazionale 5) projects n@BTF, NESCO-FI@BTF, and the AIC10-D-000570 collaboration project between INFN-Frascati (Italy) and CIEMAT (Spain).

References

[1] J. Klug, E. Altstadt, C. Beckert, R. Beyer, H. Freiesleben, V. Galindo, E. Grosse, A.R. Junghans, D. Legrady, B. Naumann, K. Noack, G. Rusev, K.D. Schilling, R. Schlenk, S. Schneider, A. Wagner, F.-P. Weiss, Nuclear Instrument and Methods in Physical Research, A 577 (2007) 641.
[2] B. Buonomo, G. Mazzitelli, F. Murtas, L. Quintieri. A wide range electrons, photons, neutrons beam facility Proceed, EPAC-2008, June 2008 23–27, Genova, Italy.
[3] B. Buonomo, G. Mazzitelli, P. Valente, IEEE Trans. Nucl. Sci. 52 (2005) 824.
[4] L. Quintieri, R. Bedogni, B. Buonomo, M. De Giorgi, A. Esposito, G. Mazzitelli, P. Valente. Feasibility Study of a Neutron sSource at the DaΦne Beam test Facility, Using Monte Carlo codes, in: 2009 IEEE Nuclear Science Symposium Conference Record, N33-6.
[5] A. Fasso et al., A Multi-particle Transport Code, CERN-2005-10 (2005), INFN/TC-05/11.
[6] D.B. Pelowitz (Ed.), MCNPX User's Manual Version 2.6, Report LA-CP-07-1473 (2008).
[7] M.B. Chadwick, P. Oblozinsky, M. Herman, et al., Nuclear Data Sheets 107 (2006) 2931.
[8] D.J. Thomas, N.P. Hawkes, L.N. Jones, P. Kolkowski, N.J. Roberts, Radiat. Prot. Dosim. 126 (2007) 229.
[9] A. Esposito, R. Bedogni, L. Lembo, M. Morelli, Radiat. Meas. 43 (2008) 1038.
[10] Z. Wang, R.M. Howell, E.A. Burgett, S.F. Kry, N.E. Hertel, M. Salehpour, Radiat. Prot. Dosim. 139 (2010) 565.
[11] R. Bedogni, P. Ferrari, G. Gualdrini, E. Esposito, Radiat. Meas. 45 (2010) 1201.
[12] R. Bedogni, A. Esposito, C. Andreani, R. Senesi, M.P. De Pascale, P. Picozza, A. Pietropaolo, G. Gorini, C.D. Frost, S. Ansell, Nucl. Inst. Meth. A 612 (2009) 143.
[13] M.J. Garcia Fusté, Neutron Spectrometry in Complex ng Fields—Application to LINAC and PET Facilities. Ph.D. thesis, Universitat Autonoma de Barcelona, Bellaterra, Spain 2010.
[14] R. Bedogni, A. Esposito, J.M. Gomez-Ros, Radiat. Meas. 45 (2010) 1205.
[15] J.M. Gómez-Ros, R. Bedogni, I. Palermo, A. Esposito, A. Delgado, M. Angelone, M. Pillon, Radiat. Meas. (2011). doi:10.1016/j.radmeas.2011.06.037.
[16] R. Boni, F. Marcellini, F. Sannibale, M. Vescovi, G. Vignola, DAFNE Linac operational performances, Proceedings of the European Particle Accelerator Conference, Stockholm, Sweden, 22–26/6/1998, p. 764; LNF-98/023(P), 27/07/1998.
[17] A. Esposito, R. Bedogni, C. Domingo, M.J. García, K. Amgarou, Radiat. Meas. 45 (2010) 1522.
[18] R. Bedogni, C. Domingo, A. Esposito, F. Fernández, Nucl. Instr. and Meth. A 580 (2007) 1301.
[19] R. Bedogni, M. Pelliccioni, A. Esposito, Nucl. Instrum. Methods A 615 (2010) 78.
[20] B. Wiegel, S. Agosteo, R. Bedogni, M. Caresana, A. Esposito, G. Fehrenbacher, M. Ferrarini, E. Hohmann, C. Hranitzky, A. Kasper, S. Khurana, V. Mares, M. Reginatto, S. Rollet, W. Rühm, D. Schardt, M. Silari, G. Simmer, E. Weitzenegger, Radiat. Meas. 44 (2009) 660.
[21] W.P. Swanson, Calculation of Neutron Yields Released by Electrons Incident on Selected Materials, SLAC-PUB-2042, November 1977.